Available online at www.sciencedirect.com
ScienceDirect
Journal of Power Sources 161 (2006) 1154–1160
JOURNAL OF POWER SOURCES
www.elsevier.com/locate/jpowsour

Electrochemical properties of the $Sm_{0.5}Sr_{0.5}CoO_3$–$La_{0.8}Sr_{0.2}Ga_{0.8}Mg_{0.15}Co_{0.05}O_3$ (LSGMC5)/LSGMC5 interface modified by an LSGMC5 interlayer synthesized using the citrate method

Shizhong Wang *, Hao Zhong, Yuman Zou

Department of Chemistry, Xiamen University, Xiamen 361005, Fujian, PR China

Received 10 April 2006; received in revised form 29 May 2006; accepted 6 June 2006
Available online 23 August 2006

Abstract

A $La_{0.8}Sr_{0.2}Ga_{0.8}Mg_{0.15}Co_{0.05}O_3$ (LSGMC5) interlayer synthesized using the citrate method was added between an $Sm_{0.5}Sr_{0.5}CoO_3$ (SSC)–LSGMC5 electrode and an LSGMC5 electrolyte pellet synthesized using a solid-state reaction, and we found that the electrode activity was improved dramatically. The SEM images of the samples demonstrated that the contact between the electrode and the interlayer was much better than the contact between the electrode and electrolyte without the interlayer. The addition of the interlayer resulted in an increased three-phase boundary length and electrode/electrolyte two-phase interfacial area. An SSC–LSGMC5 electrode sintered at 1123 K deposited onto an interlayer sintered at 1673 K exhibited the highest performance among the samples studied. The electrode resistance was about 0.08 $\Omega\,cm^2$ at near equilibrium conditions, and the cathodic overpotential at a current density of 1 $A\,cm^{-2}$ was only about 70 mV at 973 K in oxygen. The introduction of the interlayer did not change the oxygen reaction mechanism, and the significant increase in electrode performance was due to the increase in the number of active sites for oxygen reduction.
© 2006 Elsevier B.V. All rights reserved.

Keywords: Solid oxide fuel cell; Cathode; Interlayer; Oxygen reduction; Citrate method

1. Introduction

Intermediate temperature solid oxide fuel cells (ITSOFCs) are a leading technology for generating electricity in an efficient and environmental friendly process. There are growing interests in developing effective cathodes for ITSOFCs [1–4].

Strontium doped samarium cobaltite with a composition of $Sm_{0.5}Sr_{0.5}CoO_3$ (SSC) is one of the more promising cathodes for oxygen reduction [5–10]. The stability and activity of the SSC cathode can be enhanced by adding suitable amounts of LSGMC5 to the electrode [10]. However, the activity of SSC–LSGMC5 composite electrode still needs to be further improved.

It is well known that a high oxygen ionic conductivity membrane interlayer between an electrode and electrolyte could be effective in improving the performance of the electrode [11–13]. However, the mechanism is still not well understood for the improvement in electrode activity after introducing this interlayer. At present, the most often used interlayer material is doped CeO_{2-x} due to its high ionic oxygen conductivity and catalytic activity. However, SDC is not an ideal interlayer for electrodes supported on lanthanum gallate electrolytes due to the large difference in physical properties between the SDC and doped $LaGaO_3$. Considering the compatibility between the interlayer and electrolyte, an interlayer with the same chemical composition as the electrolyte could be a potential candidate. The introduction of an interlayer with the same composition as that of the electrolyte could be useful to illuminate the role of the interlayer in improving the performance of an electrode as reported in the literature, because the major difference introduced by the interlayer is the microstructure of the electrode/electrolyte interface.

* Corresponding author. Tel.: +86 592 2184968; fax: +86 592 2184968.
E-mail address: shizwang@sohu.com (S. Wang).

0378-7753/$ – see front matter © 2006 Elsevier B.V. All rights reserved.
doi:10.1016/j.jpowsour.2006.06.027

In this study, an LSGMC5 interlayer prepared using the citrate method was added between an SSC–LSGMC5 electrode and an LSGMC5 electrolyte, which improved the activity of the SSC–LSGMC5/LSGMC5 (electrolyte) interface dramatically. The synthesizing parameters were optimized, and the role of the interlayer was analyzed in detail.

2. Experimental

A $La_{0.8}Sr_{0.2}Ga_{0.8}Mg_{0.15}Co_{0.05}O_3$ (LSGMC5) electrolyte was prepared using a conventional solid-state reaction [10]. The precursors for the electrolyte were La_2O_3 (99.99%), $SrCO_3$ (99.99%), MgO (99.99%), CoO (99.9%) and Ga_2O_3 (99.99%). Powders of the precursors in a stoichiometric ratio were mixed using a mortar and pestle for 0.5 h. The mixture was calcined at 1273 K for 6 h. The calcined mixture was then isostatically pressed into a disk at 274.6 MPa for 10 min ($\phi = 2.0$ cm). The disks were sintered at 1748 K for 6 h in air. The sintered disks were polished to a thickness of about 0.3 mm. The $Sm_{0.5}Sr_{0.5}CoO_3$ (SSC)–LSGMC5 composite cathode was synthesized using the conventional solid-state reaction as reported previously [10].

LSGMC5 powder used for preparing an interlayer was synthesized using the citrate method [14]. Stoichiometric amounts of precursors were added into a beaker containing a suitable amount of concentrated nitric acid solution. After boiling for 0.5 h, an adequate amount of citric acid was added to the beaker (the molar ratio of citric acid to metal ions was about 1.25:1) under continuous heating and strong stirring until a viscous resin was formed. The mixture was then dried at around 373–393 K, and then calcined at 773 K for 2 h. Then the mixture was sintered at 1473 K for 6 h.

The electrodes were characterized using a three-electrode system as reported previously [10]. Symmetrical electrodes were prepared on both sides of an LSGMC5 electrolyte using the screen-printing method (80 mesh). SSC–LSGMC5/LSGMC5 (interlayer)/LSGMC5 (electrolyte) assemblies were prepared as follows: an LSGMC5 layer was screen-printed on both sides of an LSGMC5 electrolyte and calcined at 1573–1673 K. The SSC–LSGMC5 composite electrode was screen-printed on the calcined LSGMC5 interlayer and sintered at 1123–1223 K for 2 h. SSC–LSGMC5 electrode deposited on an LSGMC5 electrolyte without interlayer was also prepared using similar processes. The thickness of the electrode was usually about 20 μm, and the thickness of the interlayer was about 2–5 μm. Pt reference electrode was prepared on the same side of the working electrode and sintered at 1073 K for 2 h. The distance between the working and reference electrode was about 3 mm. Measurements were carried out on samples of which the impedance of the two-electrode measurement was about twice of the three-electrode measurement (within 10% error) [10,15].

All electrochemical measurements were carried out with a VMP2/Z-40 (AMETEK) electrochemical testing station. The frequency range for the impedance measurements was usually 0.01–100 kHz, and the amplitude of the input sinuous signal was 10 mV. The spent samples were examined using a scanning electron microscopy (Leo1530).

3. Results and Discussion

3.1. Effect of interlayer sintering temperature

The microstructures of various samples were examined. Shown in Fig. 1 are the SEM images of the cross-section of an SSC–LSGMC5 (1223 K)/LSGMC5 (electrolyte) interface without interlayer and SSC–LSGMC5 (1223 K)/LSGMC5 (interlayer)/LSGMC5 (electrolyte) assemblies with an LSGMC5 interlayer sintered at 1623 and 1673 K, respectively, as typical examples. The "1223 K" in the parentheses is the calcining temperature of the SSC–LSGMC5 electrode. As it can be seen from Fig. 1(a), the contact between the SSC–LSGMC5 electrode and electrolyte is relatively loose. A large blank area can be observed at the electrode/electrolyte interface.

The SEM image of an SSC–LSGMC5 (1223 K)/LSGMC5 (1623 K)/LSGMC5 (electrolyte) assembly is shown in Fig. 1(b), and the "1623 K" in the parentheses is the sintering temperature of the LSGMC5 interlayer. As can be seen from Fig. 1(b), the interlayer has a porous structure and good compatibility with the LSGMC5 electrolyte. Further, the compatibility between the SSC–LSGMC5 electrode and LSGMC5 interlayer is much better than that between the SSC–LSGMC5 electrode and LSGMC5 electrolyte without an interlayer as shown

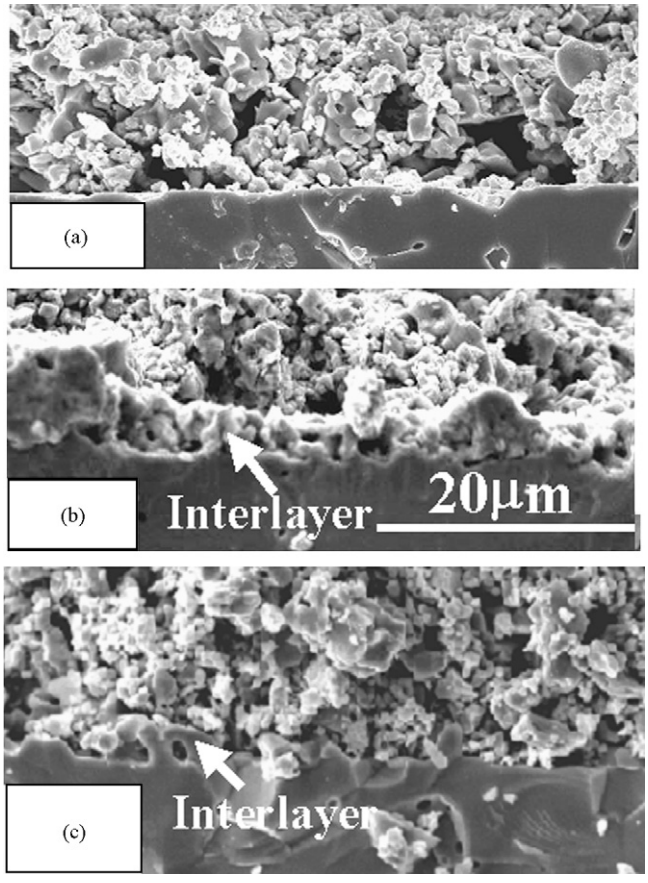

Fig. 1. SEM images of the cross-section of various samples: (a) SSC–LSGMC5 (1223 K)/LSGMC5 (electrolyte); (b) SSC–LSGMC5 (1223 K)/LSGMC5 (1623 K)/LSGMC5 (electrolyte); (c) SSC–LSGMC5 (1223 K)/LSGMC5 (1673 K)/LSGMC5 (electrolyte).

in Fig. 1(a). When the interlayer is sintered at a temperature much lower than 1623 K, the weak contact among the electrode, interlayer and electrolyte results in a poor interfacial structure. Thus, the SEM image of the SSC–LSGMC5 (1223 K)/LSGMC5 (1573 K)/LSGMC5 (electrolyte) assembly cannot be obtained, since the electrode would peel off from the electrode after the reaction.

Fig. 1(c) is the SEM image of the SSC–LSGMC5 (1223 K)/LSGMC5 (1673 K)/LSGMC5 (electrolyte) assembly. The LSGMC5 interlayer has a dense structure, and there is no obvious boundary between the interlayer and electrolyte. Furthermore, the interface between the SSC–LSGMC5 electrode and LSGMC5 interlayer is much better than that between the electrode and LSGMC5 electrolyte without interlayer shown in Fig. 1(a).

The three-phase boundary (TPB) of the SSC–LSGMC5/LSGMC5 (interlayer)/LSGMC5 (electrolyte) assembly, which is the major active reaction zone for oxygen reduction, shifts from the SSC–LSGMC5/LSGMC5 (electrolyte) interface to the SSC–LSGMC5/LSGMC5 (interlayer) interface after the introduction of an interlayer. Furthermore, the conventional electrode/electrolyte (electronic conductor/ionic conductor) two-phase interface, which is related to the transfer of oxygen ions, also shifts from the SSC–LSGMC5/LSGMC5 (electrolyte) interface to the SSC–LSGMC5/LSGMC5 (interlayer) interface. As a result, a much larger TPB length and two-phase interfacial area can be obtained after the introduction of the interlayer sintered at optimized temperature as seen from Fig. 1.

Shown in Fig. 2 are the impedance spectra at 973 K in oxygen of SSC–LSGMC5 electrodes sintered at 1223 K supported on (a) an LSGMC5 interlayer sintered at 1623 K, (b) an LSGMC5 interlayer sintered at 1673 K, (c) an LSGMC5 interlayer sintered at 1573 K, and (d) an LSGMC5 electrolyte without interlayer. The ohmic resistances of the samples can be read from the high frequency intercept of the impedance spectra, and the electrode resistances can be abstracted from the size of the impedance arcs. As it can be seen from Fig. 2, the ohmic resistance of the SSC–LSGMC5 electrode supported on an LSGMC5 interlayer sintered at 1623 K is about 0.26 Ω cm^2. This value is close to that supported on an LSGMC5 interlayer sintered at 1673 K, and it is much smaller than that supported on an LSGMC5 interlayer sintered at 1573 K and an LSGMC5 electrolyte without interlayer. Furthermore, the electrode resistance of SSC–LSGMC5 (1223 K)/LSGMC5 (1623 K)/LSGMC5 (electrolyte) assembly is only about 0.12 Ω cm^2, which is smaller than the 0.37 Ω cm^2 for SSC–LSGMC5 (1223 K)/LSGMC5 (electrolyte). Fig. 2 demonstrates that the addition of an LSGMC5 interlayer sintered at optimum temperatures can reduce both the ohmic resistance and electrode resistance of SSC–LSGMC5/LSGMC5 (electrolyte) interface dramatically.

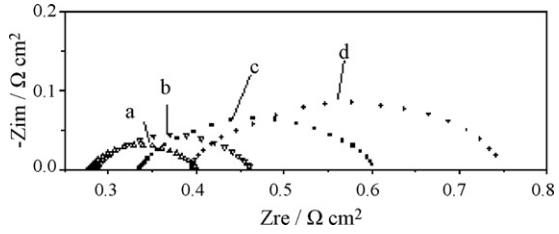

Fig. 2. Impedance spectra at OCV in oxygen at 973 K of various SSC–LSGMC5 (1223 K)/LSGMC5 (interlayer)/LSGMC5 (electrolyte) assemblies containing an interlayer sintered at (a) 1623 K, (b) 1673 K and (c) 1573 K, and (d) of an SSC–LSGMC5 (1223 K)/LSGMC5 (electrolyte) interface without interlayer.

Impedance spectra of various SSC–LSGMC5 (1223 K)/LSGMC5 (interlayer)/LSGMC5 (electrolyte) assemblies with an interlayer sintered at various temperatures were further recorded under various oxygen partial pressures and temperatures at open circuit voltage (OCV). As a typical example, the impedance spectra of SSC–LSGMC5 (1223 K)/LSGMC5 (1623 K)/LSGMC5 (electrolyte) assembly at 1073 and 973 K are shown in Fig. 3(a) and (b), respectively.

Only one major arc appears in the impedance spectra in oxygen as it can be seen from Fig. 3. With the decrease in oxygen partial pressure, another low frequency arc appears at high temperatures. At 973 K, the spectra are consisted of only one major arc even under low oxygen partial pressures (0.02 atm).

The impedance spectra can be best fitted using the equivalent circuit $LR_{el}(C(R(Q_1R_1)(Q_2R_2)))$ under low oxygen partial pressures, and using $LR_{el}(C(R(Q_1R_1)))$ in oxygen, where, L is the inductance, R_{el} the ohmic resistance of the cell and C is the interfacial capacity. Q_1 and Q_2 are constant phase elements. R, R_1 and R_2 are the resistances corresponding to the arc at high frequency, intermediate frequency, and low frequency, respectively. The R in this equivalent circuit is usually far less than 5% of the overall spectra especially at low temperatures, which corresponds to a very small arc at high frequencies in the spectra. The appearance of a small arc at high frequency in the impedance spectra is often reported in the literature [3,11]. This arc could be related to the transfer of oxygen ions since it has no dependency on oxygen partial pressure. Only arcs corresponding to Q_1R_1 and Q_2R_2 are analyzed in this study since they are the major parts of the spectra. The two arcs are defined as arc1 and arc2, respectively.

According to the Butler–Volmer equation, when the polarization overpotential is sufficiently small, i.e., $\eta \ll (RT/F)$, one can have [10]:

$$i_0 \propto \frac{T}{R_p} \quad (1)$$

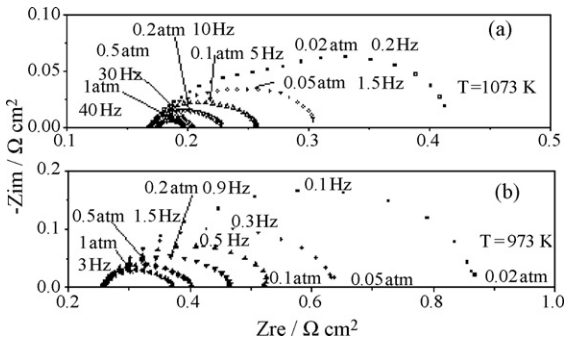

Fig. 3. Impedance spectra of SSC–LSGMC5 (1223 K)/LSGMC5 (1623 K)/LSGMC5 (electrolyte) assembly at OCV under various oxygen partial pressures at (a) 1073 and (b) 973 K, respectively.

where, η is the overpotential across the interface, i_0 the exchange current density, R_p the electrode resistance, F the Faraday's constant, R is the universal gas constant and T is the absolute temperature. From Eq. (1), it can be seen that T/R_p is proportional to exchange current density considering that the electrochemical reaction can be described using the Butler–Volmer equation. Thus, T/R_p is an important parameter for characterizing an electrochemical reaction [10].

T/R_1 and T/R_2 under various oxygen partial pressures at 1073 K of SSC–LSGMC5 (1223 K)/LSGMC5 (electrolyte) interface and SSC–LSGMC5 (1223 K)/LSGMC5 (interlayer)/LSGMC5 (electrolyte) assemblies with an interlayer sintered at various temperatures are shown in Fig. 4. It is clear that the process corresponding to arc1 has a P_{O_2} dependency of 1/2, which could be related to the surface diffusion of oxygen atom [10,16] or the dissociative adsorption of oxygen [3,7]. The P_{O_2} dependency of T/R_2 is about 1, which could correspond to the gas diffusion of oxygen. The P_{O_2} dependencies of T/R_1 and T/R_2 remain the same after the introduction of the interlayer, suggesting a similar reaction mechanism for the samples studied. Furthermore, T/R_1 increases dramatically after the introduction of an interlayer sintered at optimum temperatures. However, T/R_2 does not change after the introduction of the interlayer.

The SEM images in Fig. 1 show clearly that the addition of an LSGMC5 interlayer between the SSC–LSGMC5 electrode and LSGMC5 electrolyte increases the TPB length and the two-phase interfacial area dramatically, and this should be the major reason leading to the reduction in T/R_1. The increase in the length of TPB can lead directly to the increase in the number of active sites and reaction rate for oxygen reduction no matter the rate determining step of the reaction is surface diffusion of oxygen, charge transfer, or the dissociative adsorption of oxygen [16]. The increase in the two-phase interfacial area can improve the transfer of oxygen ions from the electrode to electrolyte, which could accelerate the overall oxygen reduction rate in case that the reaction is controlled by the transfer of oxygen ions. The increased two-phase interfacial area is also the major reason leading to the reduction of ohmic resistance for samples containing an LSGMC5 interlayer, because more part

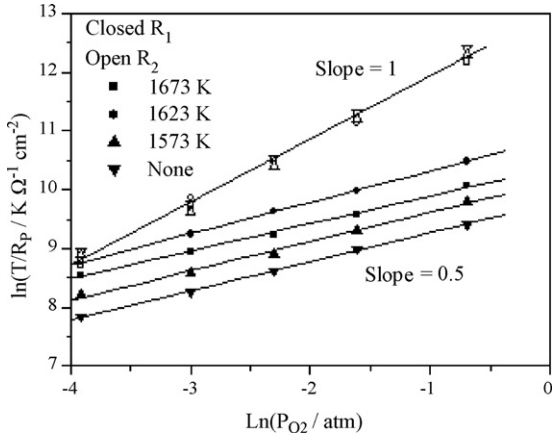

Fig. 4. T/R_1 and T/R_2 of various SSC–LSGMC5 (1223 K)/LSGMC5 (interlayer)/LSGMC5 (electrolyte) assemblies as a function of oxygen partial pressure at 1073 K.

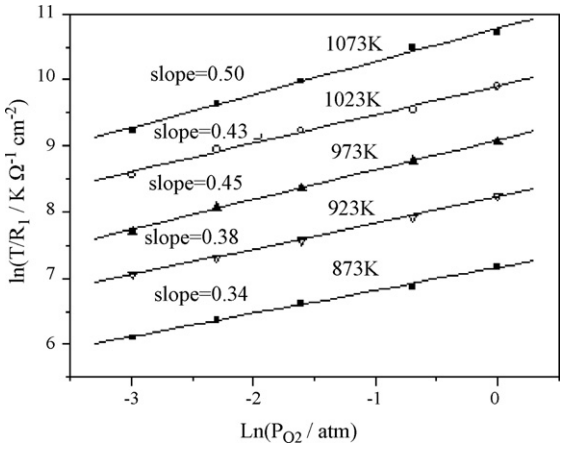

Fig. 5. T/R_1 of SSC–LSGMC5 (1223 K)/LSGMC5 (1673 K)/LSGMC5 (electrolyte) as a function of oxygen partial pressure at various temperatures.

of the electrolyte is useful for the transport of oxygen ions with the increase in interfacial contact area [17]. Arc_2 has no dependency on the electrode/electrolyte interfacial structure, because it could correspond to the gas diffusion process that is dependent on the properties of the bulk of the electrode [18,19].

The P_{O_2} dependencies of T/R_1 at various temperatures are studied. As a typical example, shown in Fig. 5 are the T/R_1 of SSC–LSGMC5 (1223 K)/LSGMC5 (1623 K)/LSGMC5 (electrolyte) assembly as a function of oxygen partial pressure at various temperatures. The P_{O_2} dependency of T/R_1 decreases from about 0.5 at 1073 K to about 0.34 at 873 K, which is similar to the behavior of an SSC–LSGMC5/$La_{0.9}Sr_{0.1}Ga_{0.8}Mg_{0.2}O_3$ interface without interlayer [10]. According to the report in Ref. [10], this result suggests that the rate determining step for oxygen reduction changes from the surface diffusion of oxygen atom or dissociative adsorption of oxygen to charge transfer with the decrease in temperature.

3.2. Effect of electrode sintering temperature

Impedance spectra at 973 K in oxygen of SSC–LSGMC5/LSGMC5 (1673 K)/LSGMC5 (electrolyte) and SSC–LSGMC5/LSGMC5 (1623 K)/LSGMC5 (electrolyte) assemblies with an electrode sintered at various temperatures are shown in Fig. 6(a) and (b), respectively. As can be seen from

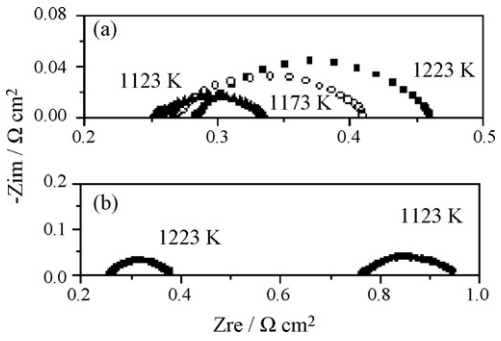

Fig. 6. Impedance spectra of electrodes sintered at various temperatures supported on an interlayer sintered at (a) 1673 K and (b) 1623 K.

Fig. 6(a), both the size of the arcs and the high frequency intercept of the spectra decrease with decreasing electrode sintering temperature. This suggests an improved electrode activity and interfacial compatibility with the decrease in electrode sintering temperature for SSC–LSGMC5/LSGMC5 (1673 K)/LSGMC5 (electrolyte) assemblies. However, the results in Fig. 6(b) show that both the size of the arcs and the high frequency intercept of the spectra increase with decreasing electrode sintering temperature for SSC–LSGMC5/LSGMC5 (1623 K)/LSGMC5 assemblies. The different effect of electrode sintering temperature on the performance of various assemblies could be due to the difference in the structure of the interlayer sintered at various temperatures. As can be seen from Fig. 1(b), the interlayer sintered at 1623 K exhibits a porous structure, which could be unstable after the addition of an electrode. Therefore, high electrode sintering temperature could be essential to obtain a stable interfacial structure.

T/R_1 and T/R_2 as a function of oxygen partial pressure at 1073 K of SSC–LSGMC5/LSGMC5 (1673 K)/LSGMC5 (electrolyte) assemblies with an electrode sintered at various temperatures are shown in Fig. 7. The P_{O_2} dependencies of T/R_1 and T/R_2 have no dependency on electrode sintering temperature, suggesting a similar reaction mechanism for electrodes sintered at various temperatures. Furthermore, the magnitude of T/R_2 also has no dependency on electrode sintering temperature, while that of T/R_1 decreases with the increase in electrode sintering temperature under various oxygen partial pressures.

The SEM images of the cross section of SSC–LSGMC5/LSGMC5 (1673 K)/LSGMC5 (electrolyte) assemblies with an electrode sintered at 1123 and 1223 K are shown in Fig. 8(a) and (b), respectively. As can be seen from Fig. 8, the change in electrode sintering temperature leads to a dramatic change in the microstructure of both the electrode and electrode/interlayer interface. The assembly with an electrode sintered at 1123 K exhibits smaller electrode particles, larger electrode surface area, and better electrode/interlayer interfacial compatibility compared with that sintered at 1223 K. Since the active reaction zone for MIEC electrodes like SSC could extend from TPB to

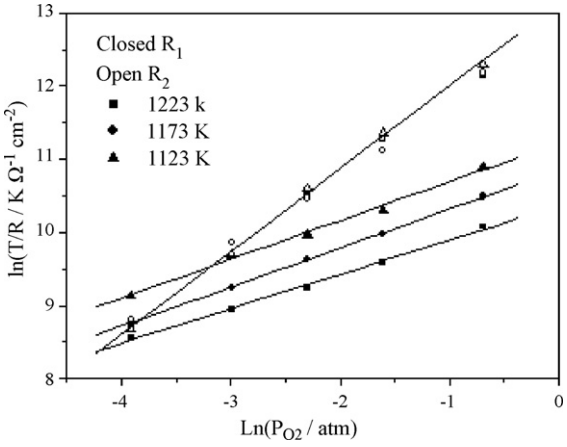

Fig. 7. T/R_1 and T/R_2 as a function of oxygen partial pressure at 1073 K of SSC–LSGMC5/LSGMC5 (1673 K)/LSGMC5 (electrolyte) assemblies containing an electrode sintered at various temperatures.

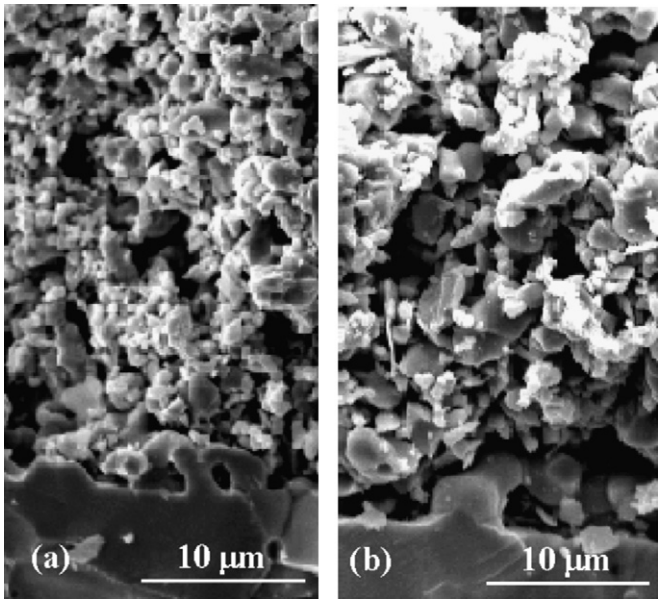

Fig. 8. SEM images of the cross-section of various samples: (a) SSC–LSGMC5 (1123 K)/LSGMC5 (1673 K)/LSGMC5 (electrolyte); (b) SSC–LSGMC5 (1223 K)/LSGMC5 (1673 K)/LSGMC5 (electrolyte).

the bulk of the electrode, both the increase in TPB length and electrode surface area will result in an increase in the number of active reaction sites and reaction rate. It is a little strange that T/R_2 is independent on the sintering temperature of the electrode, i.e., independent on the microstructure of the electrode, illustrating that this arc could correspond to a gas conversion resistance [18,19]. However, the resistance corresponding to pore diffusion through the current-collecting part of an electrode could also be independent on the microstructure of the electrode in some cases as reported in the literature [18]. Further work is still needed to address the diffusion process.

The SSC–LSGMC5/LSGMC5 (electrolyte) sample containing an electrode sintered at 1123 K has also been prepared. However, it is not stable due to the poor interfacial structure. The results in this part show clearly that the addition of an interlayer sintered at optimum conditions could modify the compatibility between the electrode and electrolyte dramatically, resulting in an improved interfacial structure and electrode performance.

3.3. Electrochemical properties of SSC–LSGMC5 (1123 K)/LSGMC5 (1673 K)/LSGMC5 (electrolyte) under high field polarization

Characteristics of various SSC–LSGMC5/LSGMC5 (interlayer)/LSGMC5 (electrolyte) assemblies as well as the SSC–LSGMC5/LSGMC5(electrolyte) interface without interlayer are studied under high field polarization. The samples show similar kinetic characteristics, and obvious Tafel regions with similar slope can be observed. As a typical example, the results of an SSC–LSGMC5 (1123 K)/LSGMC5 (1673 K)/LSGMC5 (electrolyte) assembly are discussed in detail, since it exhibits the highest performance among the samples studied.

Polarization curves at various temperatures in oxygen of SSC–LSGMC5 (1123 K)/LSGMC5 (1673 K)/LSGMC5 (elec-

Table 1
Exchange current densities and Tafel coefficients of SSC–LSGMC5 (1123 K)/LSGMC5 (1673 K)/LSGMC5 (electrolyte) and SSC–LSGMC5/LSGMC5 (electrolyte) at various temperatures in oxygen

	SSC–LSGMC5 (1123 K)/LSGMC5 (1673 K)/LSGMC5 (electrolyte)			SSC–LSGMC5/LSGMC5 (electrolyte)		
	i_0	α_a	α_c	i_0	α_a	α_c
973 K	0.366	1.2	1.2	0.077	1.0	1.0
923 K	0.173	1.2	1	0.045	1.3	1.0
873 K	0.0727	0.9	1	–	–	–

trolyte) assembly are shown in Fig. 9. The assembly shows rather high activity for oxygen reduction. For example, the overpotential at a current density of 1 A cm^{-2} in oxygen is only about 0.1 and 0.07 V at 923 and 973 K, respectively. The curves in Fig. 9 agree well with the Butler–Volmer equation (Eq. (2)):

$$i = i_0 \left[\exp\left(\frac{\alpha_a F\eta}{RT}\right) - \exp\left(-\frac{\alpha_c F\eta}{RT}\right) \right] \quad (2)$$

Here, i_0 is the exchange current density, F the Faraday's constant, R the universal gas constant, T the absolute temperature and α_a and α_c are the anodic and cathodic charge transfer coefficients, respectively.

The exchange current densities, cathodic and anodic charge transfer coefficients abstracted from Fig. 9 are shown in Table 1. For comparison, the kinetic parameters of SSC–LSGMC5 (1223 K)/LSGMC5 (electrolyte) interface are also shown in the same table. Both the cathodic and anodic charge transfer coefficients of the two samples are close to 1, illustrating a similar reaction mechanism. However, the exchange current densities of SSC–LSGMC5 (1123 K)/LSGMC5 (1673 K)/LSGMC5 (electrolyte) assembly are much higher than that of SSC–LSGMC5 (1223 K)/LSGMC5 (electrolyte) interface under the same conditions.

Polarization curves under various oxygen partial pessures at 873 K of SSC–LSGMC5 (1123 K)/LSGMC5 (1673 K)/LSGMC5 (electrolyte) assembly are shown in Fig. 10. The exchange current densities, cathodic and anodic charge transfer coefficients abstracted from Fig. 10 using Eq. (2) are shown in Table 2. Again, the cathodic and anodic charge

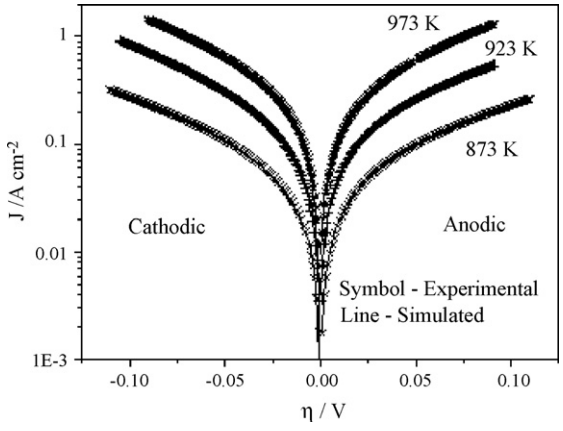

Fig. 9. Polarization curves of SSC–LSGMC5 (1123 K)/LSGMC5 (1673 K)/LSGMC5 (electrolyte) assembly at various temperatures in oxygen.

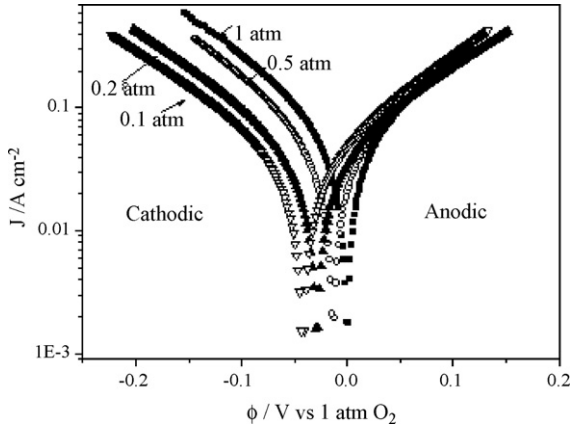

Fig. 10. Polarization curves of SSC–LSGMC5 (1123 K)/LSGMC5 (1673 K)/LSGMC5 (electrolyte) assembly under various oxygen partial pressures at 873 K.

transfer coefficients are close to 1 even under an oxygen partial pressure of 0.1 atm. The anodic current density under high overpotential shows no dependency on oxygen partial pressure. However, the cathodic current density under high overpotential increases dramatically with increasing oxygen partial pressure as it can be seen from Fig. 10.

The P_{O_2} dependencies of i_0 and cathodic current density at an electrode potential of −0.15 V referred to 1 atm oxygen are shown in Fig. 11. It can be estimated that the P_{O_2} dependency of i_0 is about 1/4, and the P_{O_2} dependency of cathodic current at an electrode potential of −0.15 V referred to 1 atm oxygen is about 1/2. This suggests that the rate determining step of oxygen reaction is charge transfer [10,20].

The results of polarization measurements demonstrate that the rate determining step for oxygen reduction over the SSC–LSGMC5/LSGMC5 (interlayer)/LSGMC5 (electrolyte) assemblies is charge transfer under high overpotential [10,20], which is the same as that of SSC–LSGMC5/LSGMC5 (electrolyte) interface without an interlayer. Taking the results at

Table 2
Exchange current densities and Tafel coefficients of SSC–LSGMC5 (1123)/LSGMC5 (1673)/LSGMC5 (electrolyte) at 873 K under various oxygen partial pressures

P_{O_2} (atm)	i_0 (A cm^{-2})	α_a	α_c
1	0.073	0.9	1
0.5	0.059	1	0.9
0.2	0.048	1	0.9
0.1	0.041	1	1

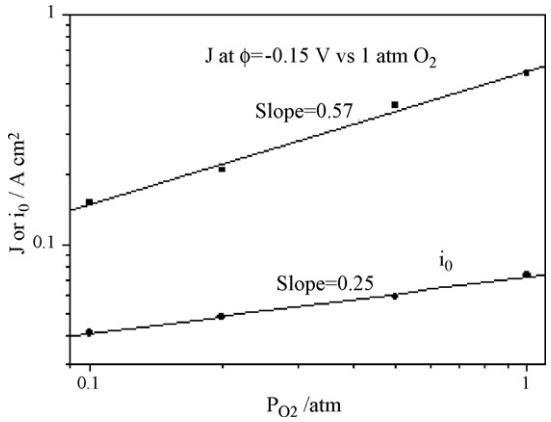

Fig. 11. Oxygen partial pressure dependencies of exchange current density and current density at −0.15 V electrode potential referred to 1 atm oxygen partial pressure at 873 K of SSC–LSGMC5 (1123 K)/LSGMC5 (1673 K)/LSGMC5 (electrolyte) assembly.

OCV into consideration, it is clear that the reaction mechanism of oxygen reduction over the SSC–LSGMC5 electrode depends strongly on the reaction temperature, oxygen partial pressure and overpotential as reported previously [10].

Because the mechanism of oxygen reduction remains the same after the introduction of an LSGMC5 interlayer between the SSC–LSGMC5 electrode and LSGMC5 electrolyte, the improved activity could be due to an increased number of active reaction sites determined dominantly by the TPB length. The results in this study show clearly the leading role of TPB in determining the electrochemical properties of SSC–LSGMC5 electrode. Furthermore, it is evident that the change in interfacial structure plays an important role in improving the performance of an electrode/electrolyte interface by adding an interlayer.

4. Conclusions

The addition of an LSGMC5 interlayer synthesized using the citrate method between the SSC–LSGMC5 electrode and LSGMC5 electrolyte increased the TPB length and the two-phase interfacial area dramatically. The addition of the interlayer has resulted in an improved electrode performance and ohmic resistance reduction. The change in interfacial structure played an important role in improving the performance of an electrode/electrolyte interface by adding an interlayer. The properties of the SSC–LSGMC5/LSGMC5 (interlayer)/LSGMC5 (electrolyte) assembly depended strongly on the sintering temperature of both the interlayer and electrode.

Acknowledgements

This material is based upon work supported by the “Fujian Province Science and Technology Program, Key Project (no. 2003H046)” and Research Fund for Homecoming Scholars.

References

[1] E.P. Murray, M.J. Sever, S.A. Barnett, Solid State Ionics 148 (2002) 27–34.
[2] V. Dusastre, J.A. Kilner, Solid State Ionics 126 (1999) 163–174.
[3] S. Wang, Y. Jiang, Y. Zhan, J. Yan, W. Li, J. Electrochem. Soc. 145 (1998) 1932–1939.
[4] Y. Jiang, S. Wang, Y. Zhang, J. Yan, W. Li, Solid State Ionics 110 (1998) 111–119.
[5] H. Fukunaga, M. Koyama, N. Takahashi, C. Wen, K. Yamada, Solid State Ionics 132 (2000) 279–285.
[6] C. Xia, W. Rauch, F. Chen, M. Liu, Solid State Ionics 149 (2002) 11–19.
[7] M. Koyama, C. Wen, T. Masuyama, J. Otomo, H. Fukunaga, K. Yamada, K. Eguchi, H. Takahashi, J. Electrochem. Soc. 148 (2001) A795–A801.
[8] H Tu, Y. Takeda, N. Imanishi, O. Yamamoto, Solid State Ionics 100 (1997) 283–288.
[9] T. Ishihara, M. Honda, T. Shibayama, H. Minami, H. Nishiguchi, Y. Takita, J. Electrochem. Soc. 145 (1998) 3177–3183.
[10] S. Wang, T. Chen, S. Chen, J. Electrochem. Soc. 151 (2004) A1461–A1467.
[11] S. Wang, Y. Jiang, Y. Zhang, W. Li, J. Yan, Z. Lu, Solid State Ionics 120 (1999) 75–84.
[12] S. Wang, T. Ishihara, Acta Phys. Chim. Sin. 19 (2003) 849–853.
[13] T. Tsai, S. Barnett, Solid State Ionics 98 (1997) 191–196.
[14] M.R. Goldwasser, M.E. Rivas, E. Pietri, M.J. Pérez-Zurita, M.L. Cubeiro, A. Grivobal-Constant, G. Leclercq, J. Mol. Catal. A: Chem. 228 (2005) 325–331.
[15] H. Hu, M. Liu, Solid State Ionics 109 (1998) 259–272.
[16] C. Schwandt, W. Weppner, J. Electrochem. Soc. 144 (1997) 3728–3736.
[17] T. Kenjo, T. Nakagawa, J. Electrochem. Soc. 143 (1996) L92–L94.
[18] S. Yoon, S. Nama, J. Hana, T. Lima, S. Hong, Solid State Ionics 166 (2004) 1–11.
[19] S. Primdahl, M. Mogensen, J. Electrochem. Soc. 145 (1998) 2431–2438.
[20] F.H. Van Heuveln, H.J.M. Bouwmeester, J. Electrochem. Soc. 144 (1997) 134–140.